Internal and external forcing of multidecadal Atlantic climate variability over the past 1200 years

Jianglin Wang[1], Bao Yang[1★], Fredrik Charpentier Ljungqvist[2,3], Jürg Luterbacher[4,5], Timothy J. Osborn[6], Keith R. Briffa[6], Eduardo Zorita[7]

[1]Key Laboratory of Desert and Desertification, Northwest Institute of Eco-Environment and Resources, Chinese Academy of Sciences, Lanzhou, China

[2]Department of History, Stockholm University, Stockholm, Sweden

[3]Bolin Centre for Climate Research, Stockholm University, Stockholm, Sweden

[4]Justus Liebig University of Giessen, Department of Geography, Climatology, Climate Dynamics and Climate Change, Senckenbergstrasse 1, D-35930 Giessen, Germany

[5]Centre for International Development and Environmental Research, Justus Liebig University Giessen, Senckenbergstrasse 3, D-35390 Giessen, Germany

[6]Climatic Research Unit, School of Environmental Sciences, University of East Anglia, Norwich, UK

[7]Institute for Coastal Research, Helmholtz-Zentrum Geesthacht, D-21502 Geesthacht, Germany

★Corresponding author: Bao Yang (e-mail: yangbao@lzb.ac.cn)

Atlantic Multidecadal Variability impacts the climate around the North Atlantic and in many other parts of the world. There are ongoing discussions on the extent to which Atlantic Multidecadal Variability is driven by external (e.g., solar, volcanic, and/or aerosol) forcing versus internal variability. Here, we provide new evidence for persistent multidecadal variability during AD 800–2010. We produce a summer Atlantic Multidecadal Variability reconstruction using a network of annually-resolved terrestrial proxy records from the circum-North Atlantic region. We find that both large volcanic eruptions and solar irradiance minima induce cool phases of Atlantic Multidecadal Variability and that both forcings together explain approximately 30% of the reconstruction variance (on timescales > 30 years). We define the Atlantic Multidecadal Oscillation as the internally-generated component of Atlantic Multidecadal Variability, and calculate it by empirically removing externally-forced variations. The Atlantic Multidecadal Oscillation reveals persistent multidecadal variability throughout the past twelve centuries, making the largest contribution to Atlantic Multidecadal Variability, and also shows coherence with Northern Hemisphere temperature variations. This attempt to quantify the internally-generated and externally-forced components of Atlantic Multidecadal Variability over more than a millennium supports further understanding of its past behavior and its role in potential decadal-scale climate predictability.

Introduction

North Atlantic sea surface temperature (SST) exhibits pronounced variability on multidecadal timescales during the last 150 years, a behavior that is commonly referred to as the Atlantic Multidecadal Oscillation (AMO)[1]. Here, we prefer the term Atlantic Multidecadal Variability (AMV) because it does not imply that it is a mode of variability generated solely by internal climate processes. The AMV affects climate of the adjacent continents[1-4], and also likely Atlantic hurricane activity[5], African Sahel drought[6], and Indian summer monsoon strength[7,8]. AMV also contributes to the multidecadal variability of Northern Hemisphere (NH) temperatures during the past 150 years[9,10], particularly in the early to mid-20th century[11]. Studies based on sea-level observations suggest that AMV is an internal mode of climate variability and is dominantly controlled by ocean circulation, primarily the Atlantic Meridional Overturning Circulation (AMOC)[12]. This is supported by model studies in which AMV-like variability can be reproduced in the absence of radiative (i.e., external) forcing and caused by the AMOC[13,14]. In contrast, other studies relegate the role of internal variability, and instead suggest that external (e.g., solar[15,16], volcanic[15,16] and aerosol[17]) forcings can modulate or even drive AMV. Even so, in those simulation studies much of the AMV-like variability, especially in the early-20th century, cannot be explained by external forcing[11,17].

Previous studies of AMV were based either on instrumental data or on climate model simulations with potential deficiencies, which limit our understanding of the long-term AMV behavior and the role of external drivers in the past. Our approach here is to first reconstruct AMV regardless of its cause, and then to subtract an empirical estimate of the externally-forced component, leaving a residual variance that may be considered to arise solely from internal variability[11,18]. It is this residual series that we define here as the AMO[11,19,20].

Reconstructing the AMV over the past 1200 years

We use 46 annually-resolved terrestrial proxy records from the circum-North Atlantic-Arctic region, Eastern North America and Europe, to reconstruct the extended summer (May–September) AMV index since AD 800 (Methods). The reconstruction was produced using a nested principal component regression (PCR) method[21] and validated using a sliding window approach for calibration and verification (Methods, Fig. 1f, Supplementary Table S2) and additionally with model-based pseudoproxy experiments (Supplementary Methods, Figs. S8–S11). A number of sensitivity tests suggest that the reconstruction is, in principle, insensitive to moderate changes in the reconstruction method or in the proxy dataset composition (Supplementary Methods). For instance, alternative reconstructions, using a reduced proxy network selected specifically or randomly (Supplementary Figs. S2, S3, S6), varying the length of instrumental calibration period or fitting to a different seasonal target (Supplementary Figs. S4, S5), or without using a nesting approach (Supplementary Fig. S7), produce multidecadal variability that is very similar to our final reconstruction.

The reconstructed summer AMV index shares 45% of the observed variance during the period 1856–2010 (Fig. 1b), increasing to 72% on decadal (>10 years) and to 88% on multidecadal (>30 years) timescales (Fig. 1c, d). The reconstructed AMV index shows cool phases in the 9th, early-14th, late-15th and 16th–19th centuries with respect to the 1856–1967 mean. Warm phases are reconstructed in the 10th–13th, early-15th and mid-late-20th centuries (Fig. 1e). The reconstructed warm phases of the AMV during the 10–13th centuries are consistent with the estimate in ref.[22] that describes the AMV as an important driver of medieval mega-droughts in the American Southwest. The reconstructed AMV exhibits multidecadal variability with dominant periodicities ranging from 64 to 88 years (Supplementary Fig. S12). Wavelet analysis[23] shows that multidecadal variability persisted throughout the past twelve centuries, with particularly strong power in the 12th–15th and 20th centuries (Fig. 2).

Our reconstruction shares similar multidecadal behaviour with two published reconstructions of the AMV[24,25] (Supplementary Figs. S13, S15), but reveals stronger and more persistent multidecadal variability (Supplementary Fig. S14). The differences between these reconstructions can be related to differences in the reconstruction method (e.g., data extracted from the climate field reconstruction approach in Mann et al.[24] versus composite-index reconstruction data as used in our study and in Gray et al.[25]), and because of the precise composition of the proxy networks. The reconstruction of Gray et al.[25] is based on a sparse tree-ring network, completely independent of our predictors; it has precise dating control, but its smaller network (only 12 sites) may compromise its representation of AMV if the centers of climate impact of AMV shift through time (also see the discussions in ref.[16]). The multi-proxy-based reconstruction of Mann et al.[24] has a good spatial coverage of proxies, partly independent of those in our network; however their inclusion of some proxy records with only decadal resolution and the separate calibration of low-frequency (<0.05 cycles/year) components reduces the degrees of freedom available for a robust calibration and verification. Our new reconstruction is based on a large number of annually-resolved, updated proxy records from the circum-North Atlantic and is validated and tested for methodological robustness using statistical and pseudoproxy tests.

External forcing and internal variability of the AMV

We performed superposed epoch analysis (SEA; Supplementary Methods, Table S3) to determine the AMV anomalies caused by solar and volcanic forcing. A superposed composite of the 15 largest volcanic eruptions[26,27] shows significant (p <0.05) negative anomalies of the AMV occur during the decade following an eruption (Fig. 3a, b). To focus on multidecadal variability, we performed similar composites but using 30-year low-pass filtered data (Fig. 3c, d). The results suggest that large volcanic eruptions were followed by about two decades of negative AMV anomalies, though the smaller sample size for the multidecadal composite yields greater uncertainties. Our result shows long-term (up to two decades) impacts of volcanic eruptions on North Atlantic SST that may be associated with interactions between atmosphere circulation, ocean circulation and sea ice[28,29]. However, an important caveat regarding the interpretation of long-term volcanic cooling in our analysis is the biological memory effects in many tree-ring width data[30] might lead to an overestimate of the persistence of volcanic cooling and an underestimate of its amplitude (this is the most numerous proxy type in our network, Supplementary Table S1). Compositing multidecadal responses to solar forcing[31,32] shows negative anomalies of AMV for about three decades following periods with weak solar forcing (Fig. 3e, f), with maximum cooling at ~17 years lag. These results suggest that the large volcanic eruptions and solar irradiance minima may both cause cool AMV phases on multidecadal timescales during the past 1200 years. However, some strong volcanic events coincide with solar minima during the past twelve centuries, further complicating the interpretation.

The cross-correlation analyses show a lagged relationship of AMV with solar and volcanic forcing (Supplementary Fig. S17), consistent with the SEA results but with stronger significance. On multidecadal timescales, the maximum correlation between the reconstructed AMV and solar forcing[31,32] is ~0.35–0.46 (p <0.05) when the AMV lags by 8–12 years, close to the lag found between solar forcing and NH temperature reconstructions[33] (also see Supplementary Figs. S18, S19). The AMV also significantly correlates with volcanic forcing[26,27] (r =~0.29–0.36, p <0.05) with approximately 6–7 years lag. Such a lagged relationship between the AMV and external forcing is consistent with climate model simulations[15] and proxy-based reconstruction[16] studies. Multiple linear regression (similar to refs[16,34]; Supplementary Methods) using these lagged relationships suggests that solar and volcanic forcing together can explain ~28% (r =0.53) of the AMV variance on multidecadal timescales (Supplementary Fig. S20). The inclusion of anthropogenic (e.g., CO_2 concentration) forcing does not improve the regression skill (Supplementary Fig. 20c, d). These results indicate that changes in both solar and volcanic forcing have affected AMV, but their linear impact contributes less than one-third of the AMV variance during the past twelve centuries.

The relationship between the AMV and external forcing might be somewhat overestimated in our reconstruction owing to our compilation of temperature-sensitive proxies, which may respond more directly to changes in external forcings. However, the response of the NH temperature to solar and volcanic forcings exhibits somewhat different patterns compared with the AMV shown in our study (see Fig. 5.8 in ref.[35]). Moreover, a recent study[36] suggests the dominant role of atmosphere and ocean circulation in controlling temperature variability in areas surrounding the North Atlantic. Thus, at least part of the impact of solar and volcanic forcing on the AMV suggested by our reconstruction may be dynamically driven (see later discussion of the difficulty in separating the internal variability from the forced component), but the internal variability and forced components are not significantly correlated (r = 0.06) during the past twelve centuries, adding credence to our separation of these components.

Similar to the approach of refs[11,19], we estimate the AMO by removing the externally-forced component from the reconstructed AMV (Supplementary Methods and Fig. S20e). The residual AMO time-series retains persistent multidecadal variations over the past twelve centuries (Fig. 2f), similar to those of the reconstructed AMV. This implies that internal processes have generated multidecadal variability of North Atlantic SST throughout the past twelve centuries, similar to the results obtained in control simulations with climate models[13,14]. Such a persistent mode of internal variability (i.e., the AMO) might be associated with ocean circulations such as the AMOC[12-14], or atmospheric circulations such as the North Atlantic Oscillation (NAO)[37-39]. However, significant multidecadal variability found in the AMO is absent in the millennium-length AMOC reconstruction[40], and the slowdown in the 20th century found in the AMOC[40] is absent in our AMO reconstruction, implying that the AMO may not be linearly associated with the AMOC.

The AMV/AMO and the NH temperature

Our new reconstruction offers an opportunity to examine the association of AMV with climate in a long-term context. We compared the reconstructed AMV with a composite of NH summer temperature-sensitive tree-ring records, using a subset from the records in ref.[41], excluding all those used in our AMV reconstruction (Supplementary Methods), and found strong support for a significant association between AMV and NH temperature at multidecadal and centennial timescales (Fig. 4).

The significant correlation arises from common variance on timescales longer than 30 years (r =0.60, p <0.001) and is still high even if the centennial timescale variance is previously filtered out (30–90 years, r =0.55, p <0.001). This strong, significant correlation does not solely arise from common external forcings: it is still significant (>30 years, r =0.47, p <0.001; 30–90 years, r =0.44, p <0.001; Fig. 4c, d) between their internal variability components, suggesting that the AMO and NH temperature are associated through internal climate variability over the past 1200 years (also see Supplementary Fig. S23).

Running correlations (150-year windows) suggest that this association between the AMV/AMO and NH temperature remains strong over most of the past twelve centuries (Supplementary Figs. S24, S25). This implies a dynamical link between the AMO and NH temperature variability during the past twelve centuries[9,11,20], and suggests that the apparent influence of AMV on regional or hemispheric climate, in a long-term context, does not arise solely from common responses to external drivers.

The findings presented here have implications for decadal-scale climate predictions, because there may be more decadal predictability in the North Atlantic than in many other regions[42]. Our longer AMV/AMO reconstructions may contribute to facilitating a better understanding of the impacts of the AMV during the pre-industrial period on the climate in North America[1,2], Europe[2,4], Asia[7,8], as well as Greenland inland ice melt[3], Atlantic hurricane activity[5], and African Sahel drought[6]. Future work should consider using climate model simulations[20] and a detection/attribution approach[43] to complement our simple approach (linear regression against forcing time-series) to separate the internal variability and forced components. Such an approach is beyond the scope of this single paper and requires multiple climate models that can realistically simulate AMV, AMO and the dynamic response of the Atlantic to external forcings on multi-decadal timescales. Our study provides a better understanding of the AMV/AMO and an improved basis for future work based on model evaluation.

References

1. Enfield, D. B., Mestas, Nuñez, A. M. & Trimble, P. J. The Atlantic Multidecadal Oscillation and its relation to rainfall and river flows in the continental U.S. *Geophys. Res. Lett.* **28**, 2077-2080 (2001).
2. Sutton, R. T. & Hodson, D. L. Atlantic Ocean forcing of North American and European summer climate. *Science* **309**, 115-118 (2005).
3. Straneo, F. & Heimbach, P. North Atlantic warming and the retreat of Greenland's outlet glaciers. *Nature* **504**, 36-43 (2013).
4. Sutton, R. T. & Dong, B. Atlantic Ocean influence on a shift in European climate in the 1990s. *Nat. Geosci.* **5**, 788-792 (2012).
5. Goldenberg, S. B., Landsea, C. W., Mestas-Nuñez, A. M. & Gray, W. M. The Recent Increase in Atlantic Hurricane Activity: Causes and Implications. *Science* **293**, 474-479 (2001).
6. Zhang, R. & Delworth, T. L. Impact of Atlantic Multidecadal Oscillations on India/Sahel rainfall and Atlantic hurricanes. *Geophys. Res. Lett.* **33**, L17712 (2006).
7. Li, S., Perlwitz, J., Quan, X. & Hoerling, M. P. Modelling the influence of North Atlantic multidecadal warmth on the Indian summer rainfall. *Geophys. Res. Lett.* **35**, L05804 (2008).
8. Wang, J., Yang, B., Ljungqvist, F. C. & Zhao, Y. The relationship between the Atlantic Multidecadal Oscillation and temperature variability in China during the last millennium. *J. Quaternary Sci.* **28**, 653-658 (2013).
9. Tung, K. K. & Zhou, J. Using data to attribute episodes of warming and cooling in instrumental records. *Proc. Natl. Acad. Sci. USA* **110**, 2058-2063 (2013).
10. Chylek, P., Klett, J. D., Lesins, G., Dubey, M. K. & Hengartner, N. The Atlantic Multidecadal Oscillation as a dominant factor of oceanic influence on climate. *Geophys. Res. Lett.* **41**, 1689-1697 (2014).
11. Steinman, B. A., Mann, M. E. & Miller, S. K. Atlantic and Pacific multidecadal oscillations and Northern Hemisphere temperatures. *Science* **347**, 988-991 (2015).
12. McCarthy, G. D., Haigh, I. D., Hirschi, J. J., Grist, J. P. & Smeed, D. A. Ocean impact on decadal Atlantic climate variability revealed by sea-level observations. *Nature* **521**, 508-510 (2015).
13. Delworth, T. L. & Mann, M. E. Observed and simulated multidecadal variability in the Northern Hemisphere. *Clim. Dyn.* **16**, 661-676 (2000).
14. Knight, J. R., Allan, R. J., Folland, C. K., Vellinga, M. & Mann, M. E. A signature of persistent natural thermohaline circulation cycles in observed climate. *Geophys. Res. Lett.* **32** (2005).
15. Otterå, O. H., Bentsen, M., Drange, H. & Suo, L. External forcing as a metronome for Atlantic multidecadal variability. *Nat. Geosci.* **3**, 688-694 (2010).
16. Knudsen, M. F., Jacobsen, B. H., Seidenkrantz, M. S. & Olsen, J. Evidence for external forcing of the Atlantic Multidecadal Oscillation since termination of the Little Ice Age. *Nat. Commun.* **5**, 3323 (2014).
17. Booth, B. B., Dunstone, N. J., Halloran, P. R., Andrews, T. & Bellouin, N. Aerosols implicated as a prime driver of twentieth-century North Atlantic climate variability. *Nature* **484**, 228-232 (2012).
18. Dai, A., Fyfe, J. C., Xie, S.-P. & Dai, X. Decadal modulation of global surface temperature by internal climate variability. *Nat. Clim. Change* **5**, 555-559 (2015).

19. Frankcombe, L. M., England, M. H., Mann, M. E. & Steinman, B. A. Separating internal variability from the externally forced climate response. *J. Clim.* **28**, 8184-8202 (2015).
20. Cheung, A. H. *et al.* Comparison of Low Frequency Internal Climate Variability in CMIP5 Models and Observations. *J. Clim.*, doi: 10.1175/jcli-d-1116-0712.1171 (2017).
21. Cook, E. R., D'Arrigo, R. D. & Mann, M. E. A well-verified, multiproxy reconstruction of the winter North Atlantic Oscillation index since A.D. 1400. *J. Clim.* **15**, 1754-1764 (2002).
22. Coats, S. *et al.* Internal ocean-atmosphere variability drives megadroughts in Western North America. *Geophys. Res. Lett.* **43**, 9886-9894 (2016).
23. Torrence, C. & Compo, G. P. A practical guide to wavelet analysis. *Bull. Amer. Meteor. Soc.* **79**, 61-78 (1998).
24. Mann, M. E. *et al.* Global signatures and dynamical origins of the Little Ice Age and Medieval Climate Anomaly. *Science* **326**, 1256-1260 (2009).
25. Gray, S. T., Graumlich, L. J., Betancourt, J. L. & Pederson, G. T. A tree-ring based reconstruction of the Atlantic Multidecadal Oscillation since 1567 A.D. *Geophys. Res. Lett.* **31**, L12205 (2004).
26. Sigl, M. *et al.* Timing and climate forcing of volcanic eruptions for the past 2,500 years. *Nature* **523**, 543–549 (2015).
27. Crowley, T. J. & Unterman, M. B. Technical details concerning development of a 1200 yr proxy index for global volcanism. *Earth Syst. Sci. Data* **5**, 187-197 (2013).
28. Swingedouw, D. *et al.* Bidecadal North Atlantic ocean circulation variability controlled by timing of volcanic eruptions. *Nat. Commun.* **6**, 6545 (2015).
29. Zanchettin, D. *et al.* Background conditions influence the decadal climate response to strong volcanic eruptions. *J. Geophys. Res.* **118**, 4090-4106 (2013).
30. Esper, J., Schneider, L., Smerdon, J. E., Schöne, B. R. & Büntgen, U. Signals and memory in tree-ring width and density data. *Dendrochronologia* **35**, 62-70 (2015).
31. Ammann, C. M., Joos, F., Schimel, D. S., Otto-Bliesner, B. L. & Tomas, R. A. Solar influence on climate during the past millennium: results from transient simulations with the NCAR Climate System Model. *Proc. Natl. Acad. Sci. USA* **104**, 3713-3718 (2007).
32. Steinhilber, F., Beer, J. & Fröhlich, C. Total solar irradiance during the Holocene. *Geophys. Res. Lett.* **36**, L19704 (2009).
33. Christiansen, B. & Ljungqvist, F. C. Challenges and perspectives for large-scale temperature reconstructions of the past two millennia. *Reviews of Geophysics* **55**, 40-96 (2017).
34. Saenger, C., Cohen, A. L., Oppo, D. W., Halley, R. B. & Carilli, J. E. Surface-temperature trends and variability in the low-latitude North Atlantic since 1552. *Nat. Geosci.* **2**, 492-495 (2009).
35. Masson-Delmotte, V. *et al.* in *Climate Change 2013: The Physical Science Basis. Contribution of Working Group I to the Fifth Assessment Report of the Intergovernmental Panel on Climate Change* (eds T.F. Stocker *et al.*) Ch. 5, 383–464 (Cambridge University Press, 2013).
36. Luterbacher, J. *et al.* European summer temperatures since Roman times. *Environ. Res. Lett.* **11**, 024001 (2016).
37. Clement, A. *et al.* The Atlantic Multidecadal Oscillation without a role for ocean circulation. *Science* **350**, 320-324 (2015).
38. Li, J., Sun, C. & Jin, F. NAO implicated as a predictor of Northern Hemisphere mean

temperature multidecadal variability. *Geophys. Res. Lett.* **40**, 5497-5502 (2013).
39. Delworth, T. L. *et al.* The North Atlantic Oscillation as a driver of rapid climate change in the Northern Hemisphere. *Nat. Geosci.* **9**, 509-512 (2016).
40. Rahmstorf, S. *et al.* Exceptional twentieth-century slowdown in Atlantic Ocean overturning circulation. *Nat. Clim. Change* **5**, 475–480 (2015).
41. Stoffel, M. *et al.* Estimates of volcanic-induced cooling in the Northern Hemisphere over the past 1,500 years. *Nat. Geosci.* **8**, 784-788 (2015).
42. Mann, M. E. *et al.* Predictability of the recent slowdown and subsequent recovery of large-scale surface warming using statistical methods. *Geophys. Res. Lett.* **43**, 3459-3467 (2016).
43. Hegerl, G. & Zwiers, F. Use of models in detection and attribution of climate change. *WIREs. Climate Change* **2**, 570-591 (2011).

Acknowledgements

B.Y. and J.W. are supported by the National Science Foundation of China (NSFC) (Grant No. 41325008, 41661144008, 41520104005 and 41602192) and the CAS "Light of West China" Program. T.J.O. and K.R.B. are supported by the UK Natural Environment Research Council (NERC, grant NE/N006348/1 and NE/P006809/1). J.L. and E.Z. acknowledge the German Science Foundation (DFG) project (Attribution of forced and internal Chinese climate variability in the common eras). B.Y., T.O. and J.L. are also supported by the Belmont Forum and JPI-Climate, Collaborative Research Action "INTEGRATE, An integrated data-model study of interactions between tropical monsoons and extratropical climate variability and extremes". F.C.L. is partly supported by a grant from the Royal Swedish Academy of Letters, History and Antiquities, and by the Bank of Sweden Tercentenary Foundation (*Stiftelsen Riksbankens Jubileumsfond*).

Author contributions

J.W. and B.Y. conceived the study, carried out the data analysis and wrote the manuscript, with contributions to the design of the study and its experiments from F.C.L., J.L., T.J.O. and K.R.B. E.Z. designed and performed the pseudoproxy experiments. All authors discussed the results, edited and commented on the manuscript.

Competing financial interests

The authors declare no competing financial interests.

Figure captions

Figure 1 | Summer AMV reconstruction. a. Location of the 46 proxy records. Colors represent the contribution (beta-weight; Supplementary Methods) of each record to the reconstruction for the most replicated nest 1500–1967 (see Supplementary Table S1 for details of each proxy record). **b.** Comparison between the reconstructed (black line; ±1RMSE, gray shading) and instrumental AMV (red line). **c, d.** As **b**, but 10-year (**c**) and 30-year (**d**) low-pass filtered. Correlation coefficient, effective degrees of freedom (N_{eff}; Supplementary Methods) and significance level during the period 1856–2010 are indicated on each panel. **e.** The AMV reconstruction for the past 1200 years (AD 800–2010), as an annually revolved reconstruction (black line; ±1 RMSE, grey shading) and 30-year low-pass filtered (red). **f.** Reduction of error (RE) and explained variance (R^2) for each nest. **g.** The number of contributing proxy records from the North Atlantic-Arctic region, Eastern North America and Europe for each nest. In each case, the AMV index is shown as anomalies relative to the 1856–1967 mean (dashed lines). The AMV reconstruction, beta-weight, R^2 and RE are reported as the median value of the 38 ensemble members derived by a sliding approach for calibration and verification in each nest.

Figure 2 | Wavelet analysis for the reconstructed AMV during the past twelve centuries. a. The annually-resolved AMV reconstruction and **b.** its wavelet power spectrum. **c**. The 30-year low-pass filtered AMV reconstruction and **d.** its wavelet power spectrum. **e.** The internal variability component of AMV (i.e., the AMO), calculated by subtracting the forced component from the reconstruction, also 30-year low-pass filtered (Supplementary Methods and Fig. S20e). **f.** The wavelet power spectrum for the AMO as shown in **e**. In all cases of Gaussian wavelet analysis, the cross-hatched region is the cone of influence, where zero padding has reduced the variance. Black contour is the 90% significance level for a red-noise (autoregressive lag1) background spectrum[23].

Figure 3 | The reconstructed AMV response to volcanic eruptions and solar variability. a. Superposed composite of the 15 largest volcanic eruptions during the past 1200 years (AD 800–2000) in the reconstruction of ref.[26]. **b.** As **a**, but using an alternative volcanic reconstruction[27]. Multidecadal composites of the 5 strongest volcanic eruptions in the reconstruction of ref.[26] (**c**) and of ref.[27] (**d**). Multidecadal composites of the 5 solar irradiation minima in the reconstruction of ref.[32] (**e**) and ref.[31] (**f**). The interannual composites were calculated using annually-resolved AMV from 5 years before to 15 years after the event year. The multidecadal composites were calculated using 30-year low-pass filtered AMV from 30 years before to 30 years after the event year. In each case, shading indicates the 95% confidence interval for the composite mean. See Supplementary Methods for the superposed epoch analysis (SEA) and Supplementary Table S3 for the selected event years.

Figure 4 | Comparison of the AMV and AMO reconstructions with Northern Hemisphere (NH) temperature. The AMV reconstruction (red) compared with a composite of 22 temperature-sensitive tree-ring records (black line, composite mean; gray shading, composite mean ±1.0 standard error) for timescales >30 years (**a**) and 30–90 years (**b**). The 22 tree-ring records are not included in the proxy dataset used in our AMV reconstruction (Supplementary Table S5). **c.** As **a**, but for the internal variability components (AMO and NH internal variability) that were calculated by subtracting the externally-forced components from the reconstructed AMV and NH temperature (Supplementary Methods, Figs. S20e, S22c). **d.** As **c**, except that the variations on timescales >90 years were filtered out. The correlation coefficient with the effective degree of freedom (N_{eff}; Supplementary Methods) and the significance level for the two compared time-series are indicated on each panel. See Supplementary Fig. S23 for an additional comparison between the AMV and a composite of 13 published NH temperature reconstructions.

Methods

Instrumental AMV index. We use a summer (May–September, MJJAS) average AMV index, computed as the area-weighted average over the North Atlantic Ocean (0–70°N), from the Kaplan SST dataset[44] as the instrumental predictand for the reconstruction. Unlike some previous studies[1,5] we do not linearly detrend this SST index to obtain the AMO index because this may introduce a biased climate signal[11]. Here we follow the approach of refs.[11,18] by reconstructing the full variation in Atlantic SST (i.e. the AMV) and then removing an estimated forced component (Supplementary Methods) to leave the internal variability, and call that the reconstructed AMO.

Selection of proxy records. The climate proxy records from the circum-North Atlantic (–100°W–35°E, 20°N–80°N), a region including the North Atlantic-Arctic region, Europe and Eastern North America (which are considered to be the centers of strong climate impacts of AMV[1-5]), were selected as the network dataset. We only retained the climate reconstructions (or proxy records used in published reconstructions) that have an annual resolution and start prior to AD 1500.

For the North Atlantic-Arctic region and Europe, temperature records (including tree-ring, ice core and historical document) used by PAGES 2k Consortium[45] were included, but superseded versions of some records were replaced by new ones, e.g., Torneträsk[46] and Jämtland[47] (Supplementary Table S1). However, we did not use any of the tree-ring network used by the PAGES 2k Consortium[45] for Eastern North America, due to weak and even negative (for part of them) correlations with temperature at annual timescales[45,48].

A number of temperature reconstructions around the circum-North Atlantic that were not included in the PAGES2k dataset were also added into our proxy dataset. In addition, a number of hydroclimate (e.g., precipitation, drought and stream flow) reconstructions for these areas were also included (Supplementary Table S1). Although the hydroclimate proxies are expected to have a less stable and more varying relationship with the AMV than the temperature proxies[49], our reconstruction was not sensitive to the inclusion or exclusion of the hydroclimate proxies (Supplementary Methods).

The final dataset comprises 46 proxy records in total, including 19 for the North Atlantic-Arctic region, 18 for Europe and 9 for Eastern North America. Details of the individual proxy records and their correlations with the AMV index are shown in Supplementary Tables S1.

AMV reconstruction. The 46 proxy records, including 35 tree-ring records, 10 ice-core records and 1 historical documentary record, were used to reconstruct an extended summer (MJJAS) AMV index. We apply the Nested Principal Component Regression (PCR) methodology[21] with a sliding window approach for calibration and verification[36,50] to the reconstruction. The nested PCR calculation was applied as follows.

Firstly, all proxy records were normalized to have zero mean and unit Standard Deviation (SD) over their common period (e.g., 1500–1967 for 46 proxy records). A principal components analysis (PCA) was calculated on the proxy predictors that have complete data for the nest period.

Secondly, the first n principal components (PCs) with eigenvalues >1 were retained as predictors for Multiple Linear Regression (MLR).

Thirdly, MLR was performed to reconstruct the AMV index by regressing the retained PCs of the proxy records against the instrumental AMV index during the calibration interval. Here, a sliding window approach for calibration and verification was used across the period 1856–1967, the maximum overlap period between the 46 proxy records and the AMV index. The initial calibration interval extends from 1856 to 1930 and was incremented by one year until reaching the final period 1893–1967, deriving an ensemble of 38 plausible reconstruction members. In each calibration step, the 37 years excluded from calibration were used for cross verification.

Finally, a nested procedure was applied by repeating the first three steps, but after removing the shortest proxy record each time.

The above PCR calculations created backward nests by considering the number of available proxies dropping back in time before AD 1500, and also forward nests by the gradually decreasing number of proxies with data after AD 1967. For each nested subset, the reduction of error (RE) and R^2 were used to assess the skill of each nested model[21].

Our method considered only the regression-based uncertainties associated with the residuals in the verification period. These were calculated as the Root Mean Square Error (RMSE) defined as:

$$\mathrm{RMSE} = \sqrt{\frac{1}{\mathrm{n}} \sum_{\mathrm{t}=1}^{\mathrm{n}} (\mathrm{y_t} - y_t')^2} ,$$

where $\mathrm{y_t}$ and $\mathrm{y_t}'$ are the actual and estimated data in year t of the verification period and *n* is the number of years during the verification period.

In each nest, the AMV reconstruction, proxy weights (Supplementary Methods), RE, R^2 and RMSE statistics (Supplementary Table S2) were then characterized as the median value of the 38 ensemble members derived by the sliding approach for calibration and verification. The final reconstruction was created by splicing together the median reconstruction and estimated uncertainties (±1 RMSE) of each nest with the maximum number of proxy records. Before splicing, the mean and variance of each nested time-series had been adjusted to be the same as the most replicated 1500–1967 nest. This approach avoids artificial changes in variance and long-term mean due to varying of available number of proxy records in each nested reconstruction[41,51].

For additional methods, see Supplementary Methods.

Data availability. The AMV/AMO reconstructions together with associated climate proxy data are archived by the National Oceanic and Atmospheric Administration (NOAA) for routine public access and use (https://www.ncdc.noaa.gov/data-access/paleoclimatology-data/datasets/climate-reconstruction).

Methods references

44. Kaplan, A. *et al.* Analyses of global sea surface temperature 1856–1991. *J. Geophys. Res.* **103**, 18567-18589 (1998).

45. PAGES 2k Consortium. Continental-scale temperature variability during the past two

millennia. *Nat. Geosci.* **6**, 339-346 (2013).

46. Melvin, T. M., Grudd, H. & Briffa, K. R. Potential bias in ‘updating’ tree-ring chronologies using regional curve standardisation: Re-processing 1500 years of Torneträsk density and ring-width data. *Holocene* **23**, 364-373 (2013).

47. Zhang, P., Linderholm, H. W., Gunnarson, B. E., Björklund, J. & Chen, D. 1200 years of warm-season temperature variability in central Fennoscandia inferred from tree-ring density. *Clim. Past* **12**, 1297-1312 (2016).

48. Trouet, V. *et al.* A 1500-year reconstruction of annual mean temperature for temperate North America on decadal-to-multidecadal time scales. *Environ. Res. Lett.* **8**, 024008 (2013).

49. Ljungqvist, F. C. *et al.* Northern Hemisphere hydroclimate variability over the past twelve centuries. *Nature* **532**, 94-98 (2016).

50. Schneider, L. *et al.* Revising mid-latitude summer-temperatures back to AD 600 based on a wood density network. *Geophys. Res. Lett.* **42**, 4556-4562 (2015).

51. Wilson, R. *et al.* Last millennium northern hemisphere summer temperatures from tree rings: Part I: The long term context. *Quaternary. Sci. Rev.* **134**, 1-18 (2016).

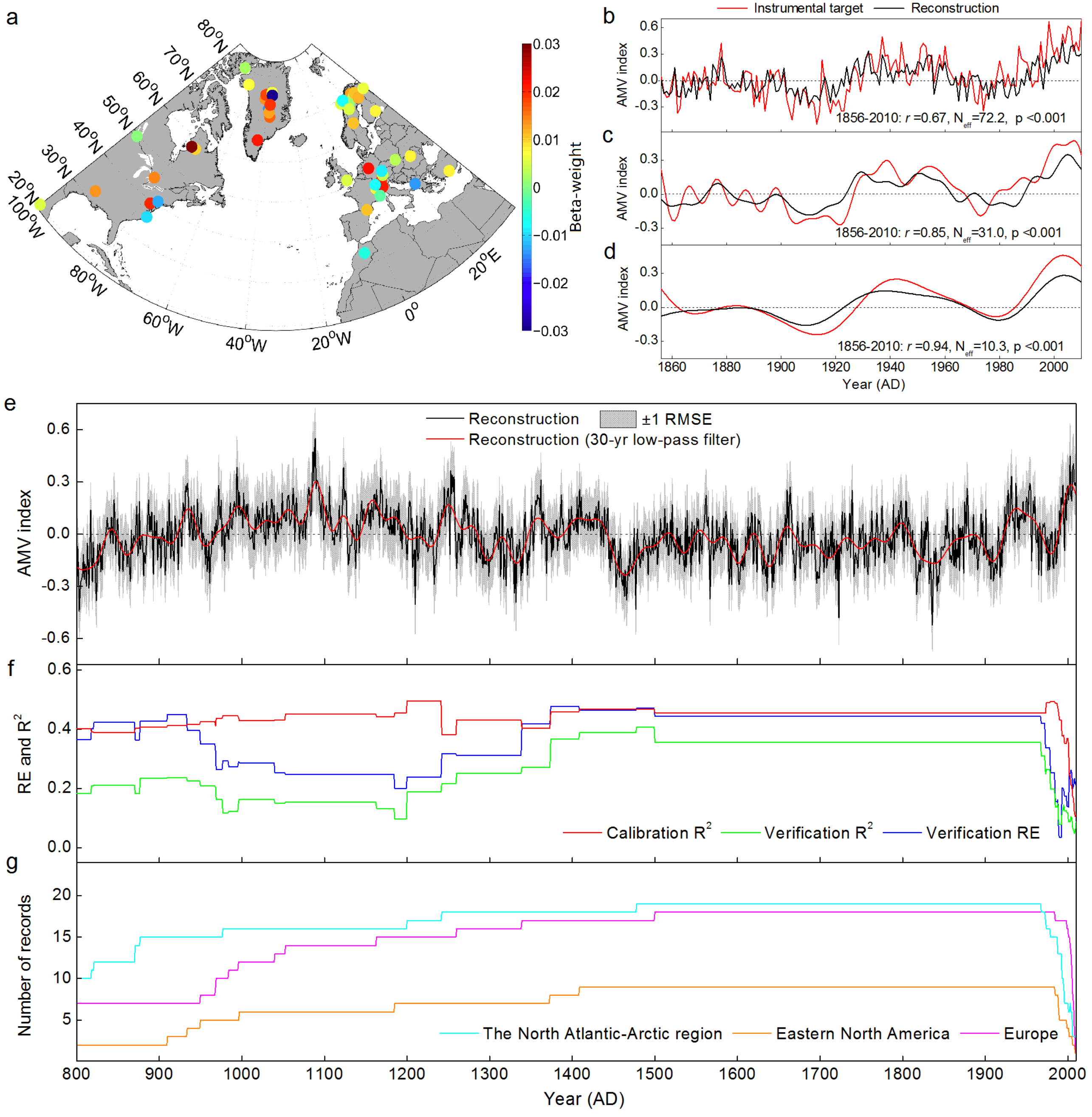
a
b
Instrumental target
Reconstruction
AMV index
1856-2010: r =0.67, N_eff=72.2, p <0.001
c
1856-2010: r =0.85, N_eff=31.0, p <0.001
d
1856-2010: r =0.94, N_eff=10.3, p <0.001
Year (AD)
Beta-weight
e
Reconstruction
±1 RMSE
Reconstruction (30-yr low-pass filter)
AMV index
f
RE and R²
Calibration R²
Verification R²
Verification RE
g
Number of records
The North Atlantic-Arctic region
Eastern North America
Europe
Year (AD)

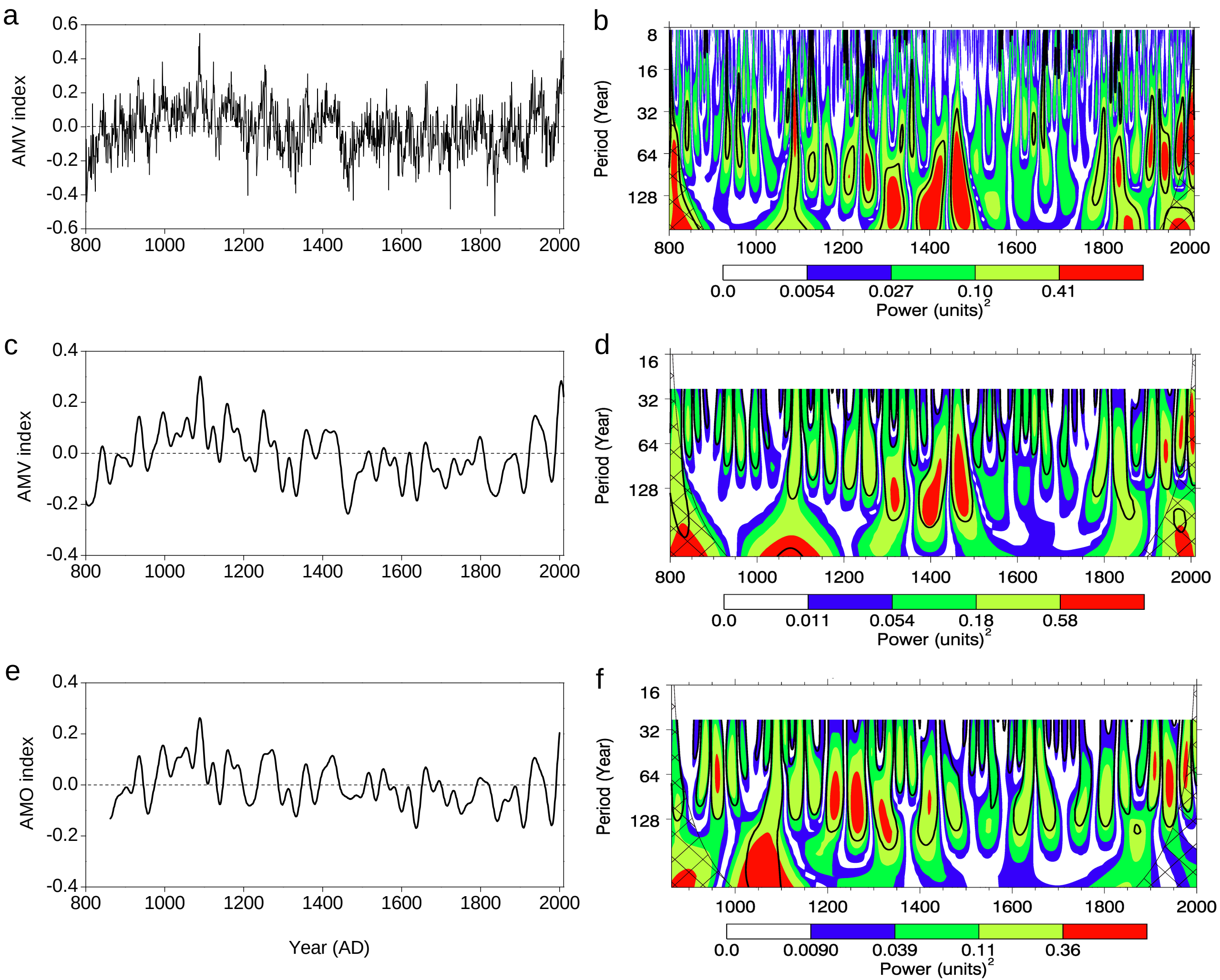

a
AMV index
0.6
0.4
0.2
0.0
-0.2
-0.4
-0.6
800 1000 1200 1400 1600 1800 2000
b
Period (Year)
8
16
32
64
128
800 1000 1200 1400 1600 1800 2000
0.0 0.0054 0.027 0.10 0.41
Power (units)^2
c
AMV index
0.4
0.2
0.0
-0.2
-0.4
800 1000 1200 1400 1600 1800 2000
d
Period (Year)
16
32
64
128
800 1000 1200 1400 1600 1800 2000
0.0 0.011 0.054 0.18 0.58
Power (units)^2
e
AMO index
0.4
0.2
0.0
-0.2
-0.4
800 1000 1200 1400 1600 1800 2000
Year (AD)
f
Period (Year)
16
32
64
128
1000 1200 1400 1600 1800 2000
0.0 0.0090 0.039 0.11 0.36
Power (units)^2

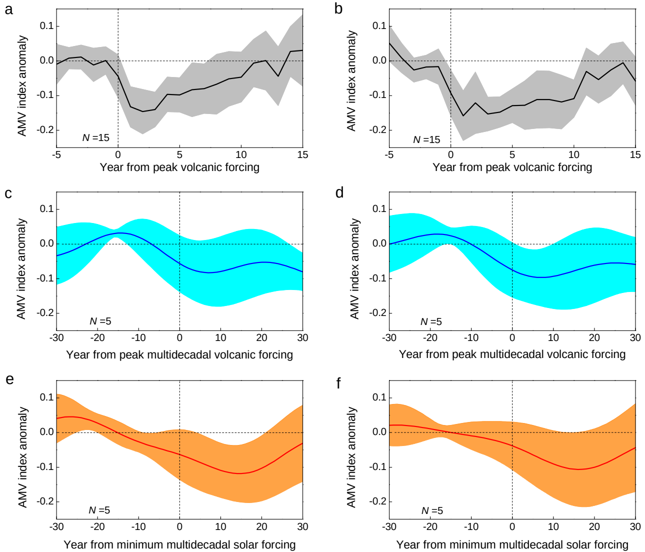
a
b
c
d
e
f
AMV index anomaly
N =15
N =5
Year from peak volcanic forcing
Year from peak multidecadal volcanic forcing
Year from minimum multidecadal solar forcing

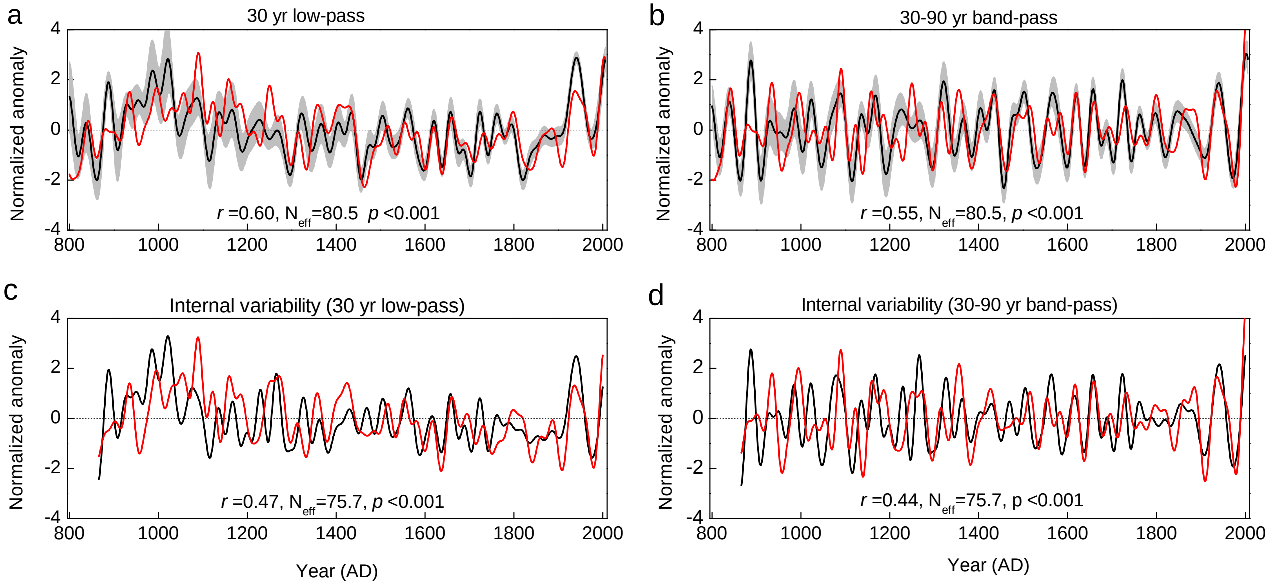
a
30 yr low-pass
r =0.60, N_eff =80.5 p <0.001
b
30-90 yr band-pass
r =0.55, N_eff =80.5, p <0.001
c
Internal variability (30 yr low-pass)
r =0.47, N_eff =75.7, p <0.001
d
Internal variability (30-90 yr band-pass)
r =0.44, N_eff =75.7, p <0.001
Normalized anomaly
Year (AD)
4
2
0
-2
-4
800
1000
1200
1400
1600
1800
2000